The Impact of Processing Parameters on the Film Solidification of Li-Ion Battery Anodes during Drying

Stefan Jaiser, Philip Scharfer and Wilhelm Schabel

Institute of Thermal Process Engineering, Thin Film Technology, Karlsruhe Institute of Technology, Kaiserstrasse 12, D-76131 Karlsruhe (Germany)

Corresponding author: stefan.jaiser@kit.edu

Presented at the 18th International Coating Science and Technology Symposium, September 19-21, 2016, Pittsburgh, PA[1]

Keywords: Drying, microstructure, film solidification, graphitic anode, Lithium-ion battery

Topic: Microstructure Development and Film Defects/Flow and Solidification of Particulate Coatings

Introduction

State-of-the-art anodes in lithium-ion batteries are typically composed of porous graphite layers that are coated on a thin, current-collecting copper foil. Their properties strongly depend on the complex microstructure, which is defined by the pore structure and the distribution of functional additives throughout the film. Polymeric binder is added in small amounts in order to provide the film with mechanical integrity, while carbon black constitutes a conductivity enhancing agent. The microstructure essentially evolves during solvent removal, which makes drying a paramount, yet insufficiently understood processing step. In the present work, an experimental approach is introduced that allows for optical evaluation of the film consolidation and the determination of the onset of surficial pore emptying. It is shown that the drying rate and the type of graphite used play a key role with regard to the film shrinkage and the onset of pore emptying.

Experimental

Materials

Anode slurries are produced through solving the polymeric binder (PVDF; polyvinylidene fluoride) and dispersing active material (Graphite) and conductive agent (carbon black) in solvent (NMP; N-Methyl-2-pyrrolidone) by means of a lab-scale mixing process. Prior to coating and drying, an optical brightener is added to the slurry in small amounts to allow for observation of the films surface during exposure to UV radiation.

Methods

Figure 1 illustrates the experimental set-up. Thin films ($d_{wet} \approx 120\ \mu m$) are cast on the copper substrate through knife coating. Solvent removal is conducted in a custom-built batch-coating and drying set-up consisting of an impingement dryer (1) and a temperature-controlled plate (2). The films dry under quasi-isothermal drying conditions as the aforementioned set-up complements the convective heat transfer by conductive heat input. At the exit of the dryer, an

[1] ISCST shall not be responsible for statements or opinions contained in papers or printed in its publications.

optical characterization module is installed, comprising a commercial SLR camera (3), a UV lamp (4) and a pressurized air nozzle (5). After a pre-defined time t_{end} that is shorter than the drying time required for solvent removal, the humid film is moved out of the dryer and stopped at a defined position beneath the camera. Three images are taken of the fluorescent film. During the second shot, a pressurized air jet is directed onto the film. This procedure is repeated for different times t_{end}.

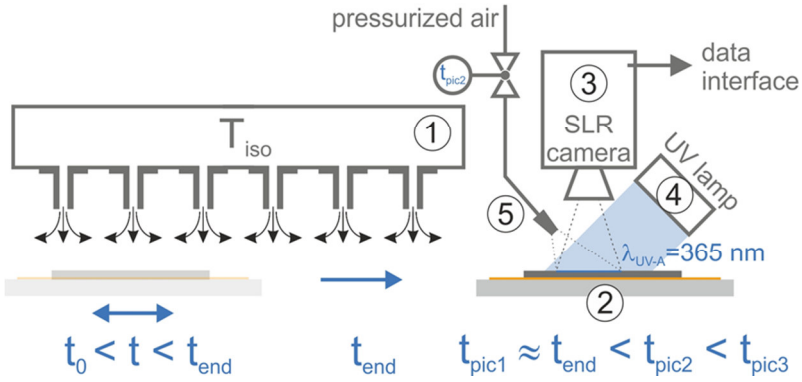

Figure 1. *Schematic illustration of the experimental setup, comprising a convective slot nozzle dryer (1), a temperature controlled plate (2) carrying the film to be dried, an SLR camera (3), a UV lamp (4) and a pressurized air nozzle (5). Subsequent to coating, the film is moved periodically beneath the array of slot nozzles. At t_{end}, the drying is stopped and the film is moved out of the dryer and stopped at a defined position beneath the camera. Three images are taken of the fluorescent film (λ_{UV-A}=365 nm). During the second shot, a pressurized air jet is directed onto the film.*

All images are evaluated by means of a simple image processing routine. The Gaussian distribution of the red channel color values of each image is determined. The color value at which the most counts are available (n_{max}) and the standard deviation of the curve (σ_n) are used for analysis. The difference of n_{max} of the first and the second image (Δn_{12}) constitutes the third characteristic quantity.

Three different scenarios are subject to research in order to study the impact of drying rate and graphite particle shape:

i.) Small, spherical graphite particles (Graphite 1) are incorporated into the slurry. The films are dried at a reference drying rate (1.2 g $m^{-2}s^{-1}$).

ii.) Large, polyhedral graphite particles (Graphite 2) are used. The films are dried under reference conditions as well.

iii.) Graphite 2 particles are used, but dried at an elevated drying rate (1.8 g $m^{-2}s^{-1}$).

Film shrinkage is investigated by means of a 2D triangulation laser.

Results and discussion

Figure 2 shows images of films that were taken after various drying times for Graphite 1 films. The first image of each three-image series is shown. Thus, the films have not been exposed to the pressurized air jet during image recording. The total drying time required for solvent removal under reference drying conditions was t_{dry}=65 s for the target dry film coating weight (m_s=72 g $m^{-2}s^{-1}$). Therefore, the images cover the entire range of drying times, with image (f) representing the dry film. The magnitude of the films fluorescent emission decreases with increasing drying time and decreasing solvent content (Figure 3 a-e). Dry films do not emit light (f). Therefore, we can conclude that the ability to emit light fluorescently when being excited by UV radiation is associated with the liquid phase of the film.

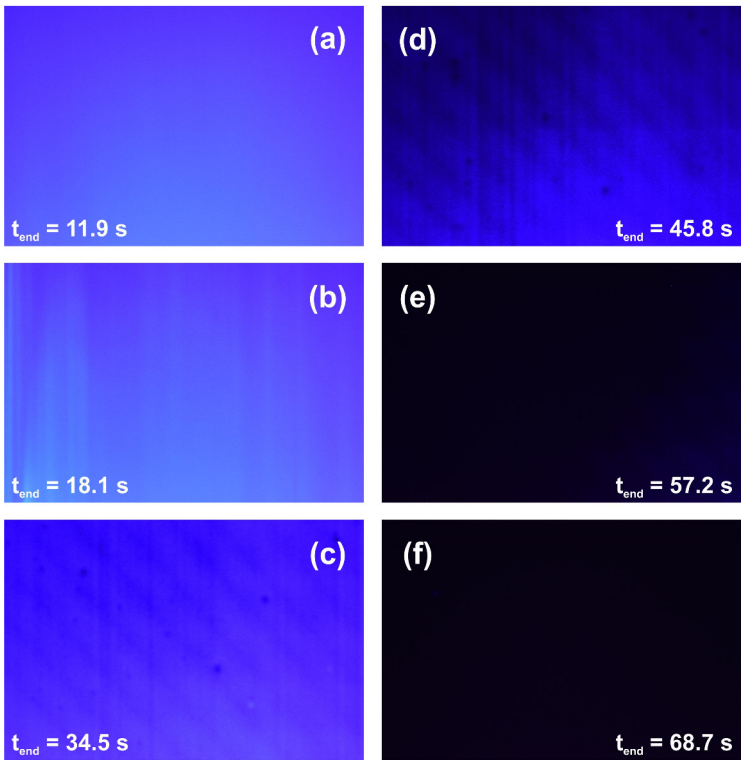

Figure 2. *RGB images captured after various drying times ranging from (a) 11.9 s to (f) 68.7 s. Three images were taken in direct succession for each t_{end}. The first image of each series is shown. The drying time of (f) exceeds the total drying time required for solvent removal (t=65 s) and therefore represents dry films. Standard drying conditions (76.5 °C, 1.2 g $m^{-2}s^{-1}$) were adjusted. The films shown were composed of the small graphite particles (Graphite 1).*

From these pictures, the characteristic quantities n_{max} and σ_n are extracted based on the image processing routine. Figure 3 illustrates the development of the Gaussian distribution of the red channel values with time. Each curve is colorized equivalent to the films appearance under exposure to UV radiation. The graph allows for assessment of the development of the two characteristic quantities σ_n and n_{max} with time. For drying times up to approximately 30 s, the mean red channel value n_{max} is about constant and the distribution is narrow. For intermediate

drying times ranging from approximately 30 to 55 s the fluorescent emission decreases with drying time. As the film approaches the dry state for drying times that exceed a distinct drying time of approximately 55 s, the Gaussians again reach a steady appearance that is characterized by narrow distributions.

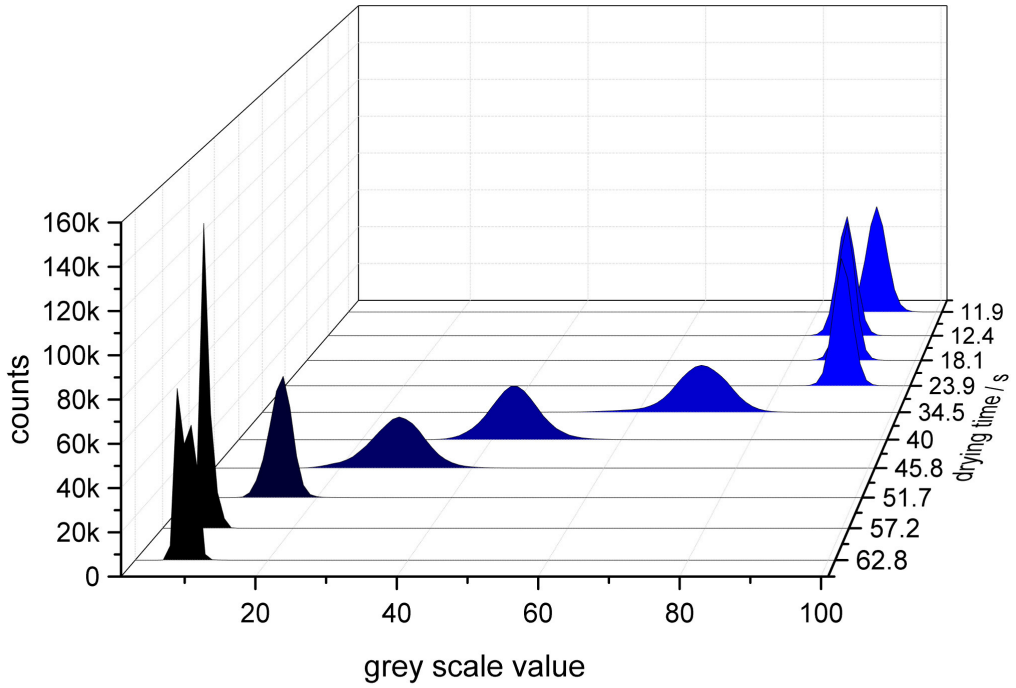

Figure 3. *Dependency of the Gaussian distribution of the grey scale value of the red channel on drying time for reference drying conditions (76.5 °C, 1.2 g $m^{-2}s^{-1}$) for a film comprised of Graphite 1. For each drying time the first image taken by the SLR camera was analyzed following the image processing routine described in the experimental section.*

From Figure 2 we have learned that the films ability to emit light is closely associated with the liquid phase. Figure 3 tells us, that within an initial time interval, this ability is not affected by evaporation-induced solvent removal. Beyond, a characteristic stage is apparent in which light emission is drastically reducing. Although the total drying time adds up to about 65 s, n_{max} is already cut into halves after 40 s. After about 55 s, no changes are visible anymore, although the film still contains significant amounts of solvent. These findings suggest that liquid that is available at the surface of the film is responsible for the appearance of the film in particular. As both graphite particles and carbon black, which are available in the film in high volumetric concentrations, are non-transparent for light in the visible spectrum, this finding is by no means surprising, but of great importance for the interpretation of the experiments.

The second information that is extracted from each trial is the difference in n_{max}, Δn_{12}, between the first and the second picture, at which the film is exposed to a pressurized air jet. Figure 4a exemplarily shows the respective images that were each taken after two different drying times. The shown images originate from the same trial that was already presented in Figure 2 and

Figure **3**. While the first film maintains its appearance during the second shot for the shorter drying time (t_{end}=12.4 s), a distinct reduction of the fluorescent emission is apparent when comparing the second with the first or third image for the extended drying time (t_{end}=40.0 s). Figure 4b depicts the Gaussian distribution of the six images. For the short drying time (t_{end}=12.4 s) all three curves exhibit similar values of n_{max}. The shifts of n_{max}, Δn_{12} and Δn_{23}, that are introduced by the air nozzle are very small and fall within the error of the experiment. In contrast, both n_{max} and the width of the curve are affected significantly by the change of the external conditions for the samples produced at t_{end}=40.0 s. Both Δn_{12} and Δn_{23} are very prominent compared to the aforementioned film.

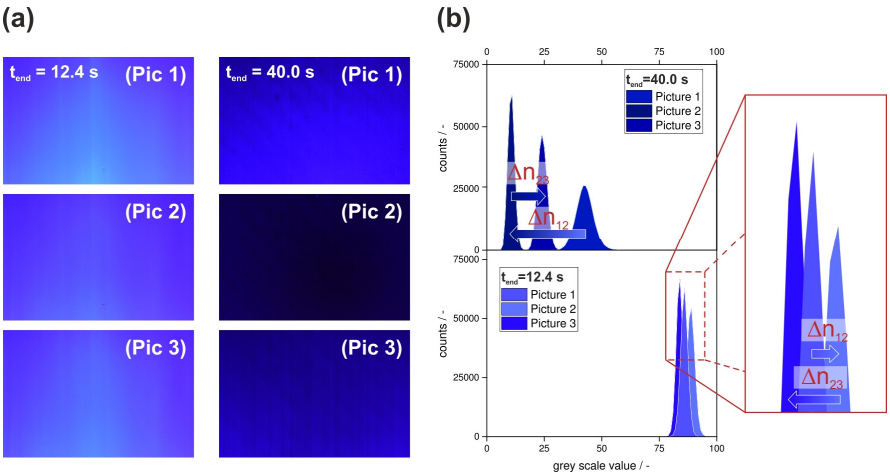

Figure 4. *(a) Comparison of the three respective images taken for each of two different drying times. During capturing the intermediate image, the film was exposed to air flow exiting the nozzle directed onto the film domain under the camera. (b) For the short drying time (t_{end}=12.4 s), high values of n_{max} are obtained for all three images taken. The shift Δn_{12} and Δn_{23} are small and fall within the range of the standard deviation of the experiments. For tend=40 s, n_{max} is significantly smaller. Operation of the nozzle results in significantly larger values for Δn_{12} and Δn_{23}.*

In the present work, the characteristic quantities n_{max}, σ_n and Δn_{12} that were introduced prior to this, are employed to illuminate the film formation of graphite anodes. The transition from the initial plateau to the characteristic, intermediate stage (Figure 3) is shown to represent the moment first surficial pores start to empty. This event can, depending on processing conditions, e.g. drying rate, or slurry properties, e.g. the employed type of graphite, occur at the moment film shrinkage is completed, but also prior to this characteristic event. The significance of this characteristic instant is discussed based on a comparison with previous findings (Jaiser et al. 2016), further emphasizing its significance.

Acknowledgements

Parts of this work were funded by the German Research Foundation (DFG, grant SCHA 1266/9-1) and the Federal Ministry of Economic Affairs and Energy (BMWI, 03ET6016) based on a

parliamentary resolution of the Deutsche Bundestag. We would further like to thank the Federal Ministry of Education and Research (BMBF) for the financial support within the cluster project “ProZell”, starting August 2016. The authors would like to thank Dr. Marcus Müller and Dr. Werner Bauer of the Ceramic Materials and Technologies department of the Institute for Applied Materials and “Project Competence E” at KIT for the close cooperation.

References

Jaiser, Stefan; Müller, Marcus; Baunach, Michael; Bauer, Werner; Scharfer, Philip; Schabel, Wilhelm (2016): Investigation of film solidification and binder migration during drying of Li-Ion battery anodes. In: Journal of Power Sources (318), S. 210–219. DOI: 10.1016/j.jpowsour.2016.04.018.